Journal of Fluids Engineering. Received May 04, 2020;
Accepted manuscript posted August 28, 2020. doi:10.1115/1.4048292

Multi-Objective Optimization of A High Specific Speed Centrifugal Volute Pump Using 3D Inverse Design Coupled with CFD Simulations

Luying Zhang
Advanced Design Technology
Dilke House, 1 Malet Street
London, WC1E 7JN, UK
l.zhang@adtechnology.com

Gabriel Davila
Franklin Electric
9255 Coverdale Road
Fort Wayne, Indiana 46809, USA
gdavila@fele.com

Mehrdad Zangeneh[1]
Department of Mechanical Engineering
University College London
Torrington Place, London, WC1E 7JE, UK
m.zangeneh@ucl.ac.uk

ABSTRACT

This paper presents three different multi-objective optimization strategies for a high specific speed centrifugal volute pump design. The objectives of the optimization consist of maximizing the efficiency and minimizing the cavitation while maintaining the Euler head. The first two optimization strategies use a 3D inverse design method to parametrize the blade geometry. Both meridional shape and 3D blade geometry is changed during the optimization. In the first approach Design of Experiment (DOE) method is used and the pump efficiency is obtained from computational fluid dynamic (CFD) simulations, while cavitation is evaluated by using minimum pressure on blade surface predicted by 3D inverse design method. The design

Journal of Fluids Engineering. Received May 04, 2020;
Accepted manuscript posted August 28, 2020. doi:10.1115/1.4048292

matrix is then used to create a surrogate model where optimization is run to find the best trade-off between cavitation and efficiency. This optimized geometry is manufactured and tested and is found to be 3.9% more efficient than the baseline with reduced cavitation at high flow. In the second approach only the 3D inverse design method output is used to compute the efficiency and cavitation parameters and this leads to considerable reduction to the computational time. The resulting optimized geometry is found to be similar to the computationally more expensive solution based on 3D CFD results. In order to compare the inverse design based optimization to the conventional optimization an equivalent optimization is carried out by parametrizing the blade angle and meridional shape.

INTRODUCTION

Centrifugal pumps have a wide range of applications in various industries. They are often used in power plants, chemical processing and municipal water supply system. Centrifugal pumps constitute a dominant portion of the world production of pumps [1], they also consume about 10% of electrical power worldwide. Good performance and high reliability of the centrifugal pumps have been actively pursued by the pump manufacturers. The hydraulic design has adopted sophisticated tools such as CFD simulations due to the late developments of the computing capabilities and advances in numerical methods [2]. Yet a fast design process that can meet many contrasting objectives remains a challenge. In many cases the impeller has to achieve both high efficiency and good cavitation performance. Structural requirements and manufacturing limits also put constraints on the hydraulic designs. An efficient design and optimization system is desired to be able to explore a large design space while providing information on the trade-offs between multiple design objectives.

Journal of Fluids Engineering. Received May 04, 2020;
Accepted manuscript posted August 28, 2020. doi:10.1115/1.4048292

A series of studies have been carried out in the past decade coupling the CFD solutions with certain optimization scheme. To reduce the computational cost, surrogate models have been widely used to approximate the response. Heo et al. [3] conducted a DOE study on a low specific speed pump with 36 design samples for 4 design variables. Impeller hub shape and blade profile and two blade angles were allowed to vary during the optimization to maximize the pump efficiency based on CFD solutions. Three different surrogate models (response surface approximation, Kriging and radial basis neural network) were investigated and the final optimized pump showed some improvement of efficiency at the design point. Tong et al. [4] carried out loss model based sensitivity analysis on a low specific speed pump to determine the key design variables. Three parameters (impeller outlet diameter, outlet width and blade outlet angle) were chosen and a design matrix of 60 samples was built with CFD solutions. Different surrogate models (quadratic response surface, the radial basis Gaussian response surface, and Kriging) were evaluated during the optimization for pump efficiency. The surrogate-CFD based approximation was more accurate than the loss model method although consumed more time. Donno et al. [5] applied Kriging and artificial neural network method to the optimization of a centrifugal pump impeller. Bezier curves are used to parameterize the meridional shape and blade profile. 16 out of 26 parameters were selected to be the design variables subject to the geometrical constraints. The DOE consists of 288 CFD solutions and single objective optimization was run to maximize the pump efficiency. The optimized design was not verified by experiments though. Wang [6] et al. optimized both the pump efficiency and the cavitation performance with an artificial neural network

Journal of Fluids Engineering. Received May 04, 2020;
Accepted manuscript posted August 28, 2020. doi:10.1115/1.4048292

model. An orthogonal design of experiments (32 samples) was designed for 8 parameters at 4 levels. The meridional shape was kept the same. Only the blade profile was optimized. Xu et al. [7] also used orthogonal method on 5 parameters to optimize the blade profile for better pump efficiency and cavitation performance. 16 samples (CFD solutions) were needed. The optimized design was selected based on orthogonal analysis. Wang et al. [8] optimized a low specific speed pump to maximize efficiency and reduce vibration. A design matrix of 15 samples for 5 parameters was built. The best solution from it was selected as the optimum design. Experimental results confirmed the improvement on both objectives. Wang [9] et al. carried out optimization on an ultra-low specific speed pump. The impeller-volute flow interaction was studied with 4 design parameters (blade outlet angle, wrap angle, volute inlet width and throat area). 9 samples orthogonal matrix was established via Taguchi method. The objectives were to reduce the entropy production and to reduce NPSHr. The matching between the impeller and volute was improved in the optimized design. Shim et al. [10] took a three-objective optimization on a centrifugal pump to reduce flow blockage at 50% of the design flow rate and to improve efficiency at design flow while reducing cavitation (NPSHr) at 125% design flow. The elementary effects method was used to select 4 key parameters (axial length of the blade, the control point for the meridional profile of the shroud, the inlet radius of the blade hub, and the incidence angle of tip of the blade). 45 design samples were generated and Kriging model was used during the optimization. Both the hydraulic performance and the reliability of the centrifugal pump were improved.

Journal of Fluids Engineering. Received May 04, 2020;
Accepted manuscript posted August 28, 2020. doi:10.1115/1.4048292

In the aforementioned studies, limited number of parameters were used in the optimization to reduce the computational cost of CFD solutions. Additional sensitivity analysis or orthogonal analysis were needed to save some computational time. Besides, the geometries of a low specific speed pump are less 3D compared to a centrifugal pump. The design space that can be covered by those selected design parameters was restricted. In this work, a multi-objective optimization strategy for a high specific speed centrifugal volute pump design is proposed. The optimization framework uses a 3D inverse design tool TURBOdesign1 [11] to generate the impeller geometries. The inverse design method uses a 3D inviscid flow solver and can solve both compressible and incompressible flow [12]. It not only generates the blade geometry but also provides an accurate 3D inviscid flow field solution, which compares well with CFD results in terms of surface static pressure. It usually computes the blade shape and the resulting flow field in a few seconds on a single core and hence can be coupled with an optimizer to explore the design space for multi-objective requirements, resulting in significant reductions in computational time versus optimization based on conventional design method coupled with 3D CFD. Another advantage of the inverse design tool lies in the way it parameterizes the blade geometry. For a 3D turbomachinery blade, a large number of parameters are usually required to describe the geometry [13], which results in a high demand on the computational resource. The inverse design method generates the blade geometry by specifying the loading parameters and enables one to represent a large design space with a few design parameters. Furthermore, the inverse design based optimization will automatically ensure that each geometry generated satisfies the required Euler head and hence it is

Journal of Fluids Engineering. Received May 04, 2020;
Accepted manuscript posted August 28, 2020. doi:10.1115/1.4048292

easy to create an accurate surrogate model based on a relatively small design matrix created by Design of Experiments method, see [14]. The surrogate model can then be used by a multi-objective genetic algorithm to trade off different objectives at multiple operating points in a few minutes.

The pump stage used for this study is a high specific speed (non-dimensional value 0.99; 407 based on rpm, m and m3/min; 2711 based on rpm, US gpm and ft) centrifugal water pump with a downstream volute. It is an existing pump designed and numerically simulated and optimized by Franklin Electric Co. Inc.. It is referred to as the 'baseline design' in this work. After verifying the performance by the laboratory test, Franklin Electric Co. Inc. manufactured and commercialized the optimized design. The discussion will start by outlining the design parameters and the methodology for the optimization of the pump impeller with the target of improving its efficiency and cavitation performance. The first approach we used is based on Design of Experiments method and the computation of efficiency by 3D RANS code, while the criterion for cavitation is taken as the minimum static pressure on blade suction surface predicted by the inverse design code. Both the meridional profile and the blade shape are parameterized. A Pareto-optimization is then carried out on the response surface to maximize the efficiency, and to minimize the cavitation. The new optimized stage (with the downstream volute retooled but kept mainly unchanged) is manufactured and its performance tested. In order to further investigate possible speedup of the optimization process, an additional optimization has been carried out based on inverse design code's outputs only for both efficiency and cavitation. In this case no CFD simulations are needed. The results show

Journal of Fluids Engineering. Received May 04, 2020;
Accepted manuscript posted August 28, 2020. doi:10.1115/1.4048292

that by carefully choosing the objectives and the constraints, it is possible to produce designs that have similar performance to the optimized design from CFD data, hence saving considerably more on the computational time. Furthermore, in order to investigate how the inverse design based optimization compares to the one based on the conventional design (where the blade geometry is parameterized without aerodynamic inputs) we show the results of an equivalent optimization for the same pump impeller by using a conventional design (ANSYS BladeModeler) based parameterization.

OPTIMIZATION METHODOLOGY

Design Constraints

The main design parameters of the pump listed in Table 1 are kept constant during the optimization work. The meridional shape can be optimized with a fixed inlet channel height (the distance between the meridional inlet shroud and hub) and a fixed impeller outlet diameter. The blade geometry has constant normal to camber line thickness at the hub and shroud. For confidentiality reason the absolute value is not given.

Optimization Framework

Figure 1 shows the general workflow of the proposed optimization scheme. This process can be fully automated under ANSYS Workbench environment or using TURBOdesign Optima [15]. A design matrix is first generated on all the parameters to be optimized. The inverse design solver then takes the inputs to produce the candidate designs. The performance of each design is evaluated by the CFD solver (ANSYS CFX) after the mesh is generated in ANSYS Meshing. From the results of CFD solution key performance data can be extracted automatically and fed into the DOE database. For the case studied the pump

Journal of Fluids Engineering. Received May 04, 2020;
Accepted manuscript posted August 28, 2020. doi:10.1115/1.4048292

efficiency, head and shaft power are computed from the CFD solutions. For the cavitation evaluation the minimum pressure on the blade surface can be extracted from the inverse design solution directly. Based on the DOE database, a response surface is built using approximation schemes (Kriging [16]). A multi-objective optimization is then run on a surrogate model within a fraction of the original computing time.

Inverse Design Method

The theory of the inverse design method was introduced in the early work [12] [17]. The tool has been applied to pump design [18] and optimization work [19] extensively. The inviscid code produces blade geometries subject to certain blade loading on the surface. The circumferentially averaged bound circulation is used as input to specify the blade loading. It is defined as:

$$r\overline{V_\theta} = \frac{N}{2\pi}\int_0^{2\pi/N} r \cdot V_\theta d\theta \tag{1}$$

The Euler head (work coefficient) can be fixed by specifying the spanwise $r\overline{V_\theta}$ distribution at the leading edge and trailing edge of the blade.

For incompressible flow the meridional derivative of $r\overline{V_\theta}$ is related to the pressure difference between the blade pressure surface and suction surface:

$$p^+ - p^- = \frac{2\pi}{N}\rho W_{mbl}\frac{\partial(r\overline{V_\theta})}{\partial m} \tag{2}$$

By prescribing the meridional derivative $\partial(r\overline{V_\theta})/\partial m$ (blade loading) in the blade passage the corresponding blade geometry can be computed by the inverse design procedure. Therefore, the blade geometry is controlled by the aerodynamic inputs which are related to the flow behavior.

Journal of Fluids Engineering. Received May 04, 2020;
Accepted manuscript posted August 28, 2020. doi:10.1115/1.4048292

Figure 2 shows the blade loading parameters required in the inverse design code to control the blade geometry. $r\overline{V_\theta}$ is normalized by the impeller outlet tip radius and speed. The normalized value ($r\bar{V}_\theta^*$) is used to specify the loading. Three segments (two parabolic curves and a linear line connecting the two) are used on the hub and shroud streamlines. Four parameters (NC, ND, SLOPE and $DRVT_{LE}$) are needed to define a loading curve. The value of $DRVT_{LE}$ ($\partial\left(r\overline{V_\theta^*}\right)/\partial m$ at the leading edge) affects the blade incidence and the peak efficiency point of the design.

Therefore only 8 parameters are needed to define a complex 3D blade shape, which greatly reduces the degree of freedom in optimization process compared to a direct design approach [20]. Furthermore, each design generated by inverse design method will satisfy the specified Euler head through the specified spanwise $r\overline{V_\theta}$. In addition, the stacking condition can be specified at a chordwise location between the blade leading edge and trailing edge. The stacking condition is used as an initial condition in the inverse design process to compute the blade shape. It is introduced by specifying variation of wrap angle from hub to tip at one quasi-orthogonal location (usually taken at trailing edge for centrifugal impellers). This can introduce an additional means of controlling the spanwise pressure field in the impeller.

Parameterization

The parameterization and the range of parameters are particularly important for optimization with expensive 3D CFD simulations. Invalid and poor designs should be filtered out before the CFD simulations are carried out. A smart parameterization as described in the inverse design method can reduce the number of design variables. Also,

Journal of Fluids Engineering. Received May 04, 2020;
Accepted manuscript posted August 28, 2020. doi:10.1115/1.4048292

it provides a visual means of inspecting the reasonable range of design parameters. For example, increasing the SLOPE value for loading to too high a value can result in region of negative loading which is not correct for a pump. Hence the range of design parameters can be set appropriately. The solver also produces candidate designs that satisfy the aerodynamic conditions and avoids unwanted designs to be passed on to CFD simulations. This improves the efficiency and effectiveness of the optimization process. In the current work both the meridional profile and the blade shape are parameterized. 17 parameters are used in total for the DOE and optimization work.

Meridional Profile Description

Figure 3 shows the parameters used to describe the meridional profile. 7 parameters are used to allow the shroud, hub, axial length and leading edge shape to vary. The LEAngle is defined as the angle between the chord of LE contour (connecting shroud and hub) and the vertical direction.

The meridional shape variation is shown in Figure 4 (the two segments at the LE are plotted to show the LEAngle) in comparison to the baseline design (blue line). The red lines show the smallest blade area and the green lines show the largest blade area. The range of the meridional parameters (relative to the baseline value) and their impact on the meridional profile can be observed in Figure 4. It can be seen that the variation of the meridional shape is quite large and the range of the parameters covers a large design space. The impeller outlet diameter is kept constant during the optimization work. It is slightly larger than the baseline design but the change in specific diameter is small. The

Journal of Fluids Engineering. Received May 04, 2020;
Accepted manuscript posted August 28, 2020. doi:10.1115/1.4048292

inlet shroud radius is allowed to vary but the channel height (the distance between the meridional inlet shroud and hub) is fixed.

Blade Profile Description

As previously mentioned, 8 loading parameters are needed to define a 3D blade geometry (Figure 2). The stacking condition is defined at the trailing edge of the blade with 1 parameter to specify the lean angle. 1 more parameter is used to vary the spanwise distribution of $r\overline{V_\theta}$. Linear distribution is used with the mean value of $r\overline{V_\theta}$ fixed to control the Euler head, but the value at the shroud is allowed to vary. In total, 10 parameters are used on describing the blade geometry. The ranges of these parameters are listed in Table 2. One important aspect of 3D optimization of pump impellers is how to set up the range of variation of parameters as widely as possible to cover a large design space but yet remain within physically realistic range. An advantage of inverse design based parametrization (based on blade loading) is that the realistic range of variation of blade loading parameters can be viewed *apriori* at the set up stage. For example, very large values of $SLOPE_{hub}$ parameter could lead to negative blade loading which is not realistic. This helps designers set the range of parameters as wide as realistically possible and hence avoid the situation where many designs fail in CFD meshing or CFD computations.

CFD METHODOLOGY

In the workflow described in Figure 1, ANSYS CFX (19.2) is used in all the CFD simulations. It uses an element-based finite volume method and a pressure-based coupled solver approach. The solution variables and fluid properties are stored at the nodes (mesh

Journal of Fluids Engineering. Received May 04, 2020;
Accepted manuscript posted August 28, 2020. doi:10.1115/1.4048292

vertices). A high resolution advection (2nd order accuracy) is used with SST turbulence model. A tri-linear element shape function is employed to interpolate diffusion term and a linear-linear interpolation shape function is used for pressure gradient terms.

For the DOE data generation, the CFD calculations are performed on the impeller domain only (single passage) under the single phase steady state assumption. The working fluid is water. Total massflow is specified at the inlet and static pressure is specified at the outlet. Rotational periodic boundary condition is given in the circumferential direction. For the wall surface, no-slip wall boundary condition is specified with a roughness of 0.02 mm. For steady state calculation, a frozen-rotor method is used at the interface between the rotating and stationary domains. No leakage flow is simulated in the CFD calculations. The convergence criteria were the root-mean-squared (RMS) residual for the continuity and momentum equations in the computational domain. For the non-cavitating conditions at the design conditions, when the solutions were converged the RMS residual values were less than 7e-5.

An unstructured tetrahedral mesh with prism layer near the wall is used for the impeller passage. For a single passage the mesh size is around 400,000 tetrahedral elements with 16 layers at wall boundary. The Y+ value is around 10. A mesh sensitivity study has been done (on an impeller geometry from the DOE database) by refining the mesh to different densities. Table 3 shows the three levels of mesh density used in the study. All have Y+ value below 10. The finer level mesh element number tripled that of the coarser level mesh. The difference of the normalized head between the finest mesh and the coarsest mesh is around 0.3%. The result of the medium mesh converges to that of the fine mesh.

Journal of Fluids Engineering. Received May 04, 2020;
Accepted manuscript posted August 28, 2020. doi:10.1115/1.4048292

Figure 5 shows the blade surface mesh distribution of the three meshes. The sensitivity study shows that the coarse mesh produces similar trend compared to the refined mesh. For the DOE study the coarse mesh from Table 3 (Figure 5, upper) is adopted in the simulations to allow a large database to be built with moderate computational resource. When the final design was selected from the optimization process the performance has been checked on the medium mesh (Figure 5, middle).

For the cavitation performance evaluation two phase flow simulation (homogeneous assumption) is carried out. The working fluid is considered as a mixture of the water and vapor at 25°C. Rayleigh Plesset cavitation model is adopted for cavitating flow with saturation pressure set to 3175 Pa and the mean diameter of nucleation site 2 μm. The inlet total pressure was initially specified as 1bar, and then gradually reduced to obtain a suction performance curve. For the final selected design, transient simulation is performed on the whole stage domain (inlet duct, impeller and volute) under two phase flow assumption. Figure 6 shows the computational domain and the mesh detail. The total mesh size is around 2,160,000 tetrahedral elements. For the transient simulation the whole annulus domain is used for the impeller and transient rotor-stator interface (sliding interface) is applied between the rotating domain and the stationary domain. The time marching scheme (second order backward Euler scheme) covers 1 degree per time step. 10 revolutions time has been covered in the simulation. The inner loop takes 10 iterations maximum and a convergence criteria of RMS residual less than 6e-5 has been used.

RESULTS

Design of Experiments

Journal of Fluids Engineering. Received May 04, 2020;
Accepted manuscript posted August 28, 2020. doi:10.1115/1.4048292

Using the algorithm described before a DOE is carried out first. The design matrix is generated using Optimal Space-Filling method. 217 CFD solutions have been collected for the 17 design parameters. The solutions contain the impeller domain only and no leakage flow or disk friction is considered in the simulations. Figure 7 shows the total to total efficiency and head of the impeller extracted from the CFD data (normalized by the baseline impeller head). It can be seen that the efficiency of all the 217 solutions is above 90%, which means the candidate designs are of good quality. The head produced by the impeller is increasing with the efficiency. But most of the points are within 10% variation of the baseline head value.

For the cavitation evaluation the minimum pressure on the blade surface (Pmin) has been extracted from all the inverse design solutions. For a given design higher Pmin value means the cavitation is less severe. Figure 8 shows the efficiency and Pmin for the 217 designs. It can be observed that for the high efficiency designs Pmin is not necessarily high, which means the cavitation may be heavy. To optimize for contrasting objectives (efficiency vs cavitation) a Pareto-optimization should be adopted.

The value of Pmin is not only an indicator of the cavitation inception but also correlates well with the head drop performance when the passage flow is not dominated by flow separation. Because the value of the minimum static pressure on the blade surface is closely related to the pressure field in the surrounding region, which is the driving factor of flow cavitation. To verify this, three designs of different Pmin values (-60, -38 and -23 Pa) are picked from the high efficiency front of the DOE data. The three points are also marked in Figure 8. The head drop curves of the three designs are produced by two-phase

Journal of Fluids Engineering. Received May 04, 2020;
Accepted manuscript posted August 28, 2020. doi:10.1115/1.4048292

flow simulations at 115% design flow rate, since the pump operation is vulnerable to cavitation at higher flow rate. The results are shown in Figure 9. The three designs produce similar impeller head at the design condition, which is used to normalize the plot. The NPSH value is normalized by the suction head at which no cavitation is triggered in the impeller. The comparison shows that as Pmin is increased the NPSHr value (NPSH for 3% head drop) is reduced. The value of Pmin predicted the right trend of suction performance change.

Multi-Objective Optimization

Based on the DOE data collected, a response surfaces is built using Kriging approximation. A multi-objective optimization is carried out on the response surface. As the turbomachinery design optimization is a multi-peak problem (due to the strong non-linearity), a genetic algorithm optimizer has been applied. The objectives are to maximize the efficiency, Pmin and power (and therefore maximize the head). Figure 10 shows the pareto front of the optimization on the response surface (red dots). After the optimization a final design (green dot) is picked from the DOE & optimization data collection subject to some manufacturing limitations (investment casting process in which the curvature of the blade and the variation of the blade wrap angle has some limitations). Figure 11 shows the comparison between the optimized design and a baseline design. It can be observed that the optimized design (red) has increased the shroud curvature and delayed the flow turning compared to the baseline design (green). The leading edge curvature has also been increased.

Journal of Fluids Engineering. Received May 04, 2020;
Accepted manuscript posted August 28, 2020. doi:10.1115/1.4048292

The loading distribution of the two designs has also been compared to each other in Figure 12. The baseline design has very high $DRVT_{LE}$ at both the hub and the shroud, which means there is strong positive incidence on the impeller blade. The optimized design reduced the $DRVT_{LE}$ significantly; as a result, the positive incidence is also reduced.

The impact of changing the loading distribution can be visualized in Figure 13. The suction surface static pressure contours (at design point) show that the low pressure zone at the blade leading edge is much smaller in the optimized design (right). As this region is where the cavitation initiates (due to the low pressure) the optimized design should reduce cavitation in the impeller passage. This has been verified by both two-phase flow CFD simulation and the laboratory test.

The two-phase CFD simulation is performed on the whole stage domain (inlet duct, impeller and volute). Figure 14 shows results of the two-phase flow simulation at 115% design flow rate, since the pump operation is vulnerable to cavitation at higher flow rate. The iso-volume captures the region where the vapor fraction is above 0.01%. It is very obvious that the baseline design experiences cavitation at such condition while the optimized design does not. This confirms the cavitation reduction effect due to the improved surface pressure distribution predicted by the single phase simulation.

The whole new stage including volute was then manufactured and tested in the Franklin Electric facilities. Figure 15 shows the prototype of the optimized design. The volute was retooled with a splitter at the outlet pipe of the volute removed. The rest of the geometry was kept unchanged. The matching between impeller exit flow and volute inlet flow was not affected. The test followed the standard specified in [21]. The instrument error is

Journal of Fluids Engineering. Received May 04, 2020;
Accepted manuscript posted August 28, 2020. doi:10.1115/1.4048292

±0.5% and the randomness is ±0.5%. The performance data from the laboratory test that cover a wide operating range (20% to 115%) are shown in Figure 16. The 4th order polynomial is used in curve fitting. The head values are normalized by the baseline value at the design point. The efficiency numbers are normalized by the peak efficiency value. It can be observed that the optimized design produces a similar head to the baseline design at most conditions, but a much higher head at around 115% design massflow. This is due to the reduction on cavitating flow under such conditions, which is captured by the two-phase flow CFD simulation as shown in Figure 14. In addition, the test data show an improvement of efficiency in general by the optimized design. At the design flow condition, the laboratory test data shows that the optimized design has an efficiency improvement of 3.9%. This is due to the improvement on cavitation performance and the reduction on passage flow loss.

The measured suction performance characteristics are shown in Figure 17. The NPSHr value (NPSH for 3% head drop) is normalized by the baseline value at the design point. The reduction on cavitation can be confirmed by the NPSHr curve, which shows that a lower NPSHr value is produced by the optimized design in comparison to the baseline design, especially towards the high flow rate conditions. It is consistent with the higher head and efficiency observed for the optimized design at such conditions in Figure 16.

Optimization Based on Inverse Design Flow Field

The results from the automated optimization based on inverse design code coupled with CFD solutions show a big improvement on pump performance over the baseline design. Yet, it is of great interest to further investigate the possibility to use inverse design flow

Journal of Fluids Engineering. Received May 04, 2020;
Accepted manuscript posted August 28, 2020. doi:10.1115/1.4048292

field solution only in the optimization. This will significantly save the computational resource and time spent on collecting/post-processing the CFD solutions. As described before, Pmin has been extracted from inverse design solutions to evaluate the cavitation potential. It will still need some performance data to evaluate the efficiency of a given design. To maximize the impeller efficiency two more parameters from inverse design code are used as objectives. The first one is the profile loss factor. The data from DOE (Figure 18) shows it has a strong correlation with the impeller efficiency. The profile loss factor is computed from the integration of cube of blade surface velocity, predicted by the inverse design code. Previous work [22] shows that the entropy generation on the blade surface is largely proportional to this value:

$$\dot{S} = \int_0^x \frac{\rho V_\delta^3 C_d}{T_\delta} dx \qquad (3)$$

The trend in Figure 18 suggests that for this current design the efficiency is sensitive to the friction loss generated on the blade surface. To achieve high efficiency the profile loss should be minimized.

The second parameter is the secondary flow factor. Secondary flow loss contributes a big portion of the total passage loss in a centrifugal machine. It also has a big impact on the 'jet-wake' flow exiting the impeller [22] [23]. Secondary flow factor is characterized by the loading difference between the hub and the shroud. It is calculated in the inverse design code by using the velocity difference (downstream of 50% streamwise location) between the hub and the shroud of the blade. It is a parameter corresponding to the hub-to-shroud secondary flow, which moves low momentum (high entropy) fluid to the shroud suction corner and contributes to the 'wake'. Suppressing this radial flow in the

Journal of Fluids Engineering. Received May 04, 2020;
Accepted manuscript posted August 28, 2020. doi:10.1115/1.4048292

impeller passage will reduce the loss associated with the secondary flow and the non-uniform exiting flow. Figure 19 shows the flowchart of the optimization using the inverse design solver only. Since no CFD data is needed the optimization work can be carried out within TURBOdesign Suite [24] using its embedded genetic optimizer (TDOptima). A direct optimization can be carried out since the turnaround time for each inverse design solution is only a few seconds.

Two constraints are set to rule out the invalid designs. The throat variation is ±2.5% of the previous design and the diffusion ratio is constrained to avoid flow separation. Table 4 shows the constraints and objectives used in the optimization. The parameterization and the ranges of the parameters are the same as the DOE work.

In total, 868 feasible inverse design solutions have been collected. The results are plotted in Figure 20. The colour and size of the bubble represent Pmin. The darker and bigger bubbles have higher Pmin value and therefore are less likely to cavitate. It is very obvious that minimizing profile loss and minimizing secondary flow are contrasting objectives and a Pareto front of the two objectives can be observed. However, when considering the cavitation performance, the designs of low profile loss and low secondary flow (therefore high efficiency) can have a bigger potential to cavitate. There is also contrast between high efficiency and low cavitation. The optimizer can filter out the points on the Pareto front for the three objectives. From these points a final design (marked by the black bubble) is selected in the high efficiency zone with modestly low cavitation. It is denoted as TD1 optimized design.

Journal of Fluids Engineering. Received May 04, 2020;
Accepted manuscript posted August 28, 2020. doi:10.1115/1.4048292

The meridional geometry of the TD1 optimized design is compared to the CFD optimized design in Figure 21. The TD1 optimized design further increases the curvature of the shroud and hub profile and slightly reduces the outlet width.

The loading distributions of the two designs are shown in Figure 22. The TD1 optimized design further reduces $DRVT_{LE}$ at the shroud to maximize Pmin. Meanwhile the hub is aft-loaded to reduce the pressure difference between the hub and shroud. This type of loading distribution has an effect of suppressing the secondary flow in the centrifugal machines [17].

Figure 23 shows the impact of loading distribution on the flow pattern. The blade suction surface streamlines are plotted for both the CFD optimized design and the TD1 optimized design. It can be observed that the radial flow movement is suppressed in the latter and the suction-shroud corner separation is reduced.

In addition, an aerodynamic blockage factor can be computed at the impeller trailing edge as a measure of the non-uniformity of the exiting flow. The blockage factor is defined as the ratio of the area-averaged (circumferentially) meridional velocity to the mass-averaged meridional velocity. A number that is closer to 1.0 means circumferentially more uniform flow distribution. Figure 24 shows the spanwise distribution of the blockage factor for the CFD optimized design (blue) and the TD1 optimized design (red). It can be observed that the exiting flow uniformity is improved for the TD1 optimized design, due to the suppression of secondary flow in the impeller passage.

The static pressure distribution on the blade suction surface can be visualized in Figure 25. The comparison shows that the low pressure zone at the blade leading edge is further

Journal of Fluids Engineering. Received May 04, 2020;
Accepted manuscript posted August 28, 2020. doi:10.1115/1.4048292

reduced in the TD1 optimized design (right) due to the smaller incidence at the shroud. Therefore, this design should also be able to reduce the cavitation zone seen at the impeller blade leading edge in the baseline design, which has been shown in Figure 14, left. Again, two-phase flow CFD simulation has been carried out to verify this. Figure 26 shows results of the two-phase flow simulation at 115% design flow rate on a single passage domain. The iso-volume shows the region where the vapor fraction is above 0.01%. It confirmed that the TD1 optimized design also has no cavitation at this condition. Finally, the performance of the TD1 optimized design is compared to that of the CFD optimized design in Figure 27. The head is normalized by the baseline design head at 100% flow condition. It can be seen that the two designs have similar efficiency at 85%, 100% and 115% flow rate. The head produced by the TD1 optimized design is slightly lower but it is still higher than the baseline design. This confirms that by minimizing the profile loss and the secondary flow loss it is possible to optimize the design efficiency and achieve good head performance.

DOE with Conventional Design Approach

In order to compare the inverse design based DOE with the conventional design (direct design) based DOE the same work was repeated this time with ANSYS BladeModeler. In ANSYS BladeModeler three camberlines (at shroud, midspan & hub) are used to parameterize a 3D impeller blade. Each camberline is described with 4 Bezier control points, as shown in Figure 28. The control points position is fixed along the % M-Prime. At each point the beta angle (with respect to the tangential direction) is allowed to vary. The LE and TE blade angle are allowed to vary by ± 10 degrees. The points at 12.5% and

Journal of Fluids Engineering. Received May 04, 2020;
Accepted manuscript posted August 28, 2020. doi:10.1115/1.4048292

50% of %M-Prime are allowed to vary by ± 20 degrees. These values were carefully selected to be consistent to the range exhibited by the CFD and inverse design flow field solution optimizations. The meridional profile is parametrized and controlled within the same range as described in Figure 3 & Figure 4.

Two sets of DOE have been carried out using ANSYS BladeModeler. ANSYS CFX with the same computational mesh and boundary conditions as described earlier was used to compute the key performance parameters, efficiency and Pmin (minimum static pressure on blade surface). The results are shown and compared to the inverse design based DOE data in Figure 29 and Figure 30. Figure 29 shows the comparison of head versus Pmin for different DOEs. The first set of DOE (grey points) has no constraint on the blade angle at the trailing edge; while the second set (yellow points) fix the trailing edge blade angle. It can be observed that with the blade angle constrained at trailing edge the impeller head is better controlled (less points with very low head). However, when compared to the inverse design based DOE data the impeller head is still scattering over a wide range (±20 of baseline value for conventional design versus less than 10% variation for inverse design DOE). The inverse design shows a much tighter control on head and the values of Pmin are relatively high. This helps to create an accurate surrogate model that automatically cover the correct part of the design space. In contrast the conventional DOE surrogate model had poor accuracy, because of large variation in head.

The comparison of the efficiency in Figure 30 for the different DOEs also shows how the inverse design based optimization concentrate the DOE points in areas of high efficiency as compared to the direct design based parameterization of the blade shape. It is very

Journal of Fluids Engineering. Received May 04, 2020;
Accepted manuscript posted August 28, 2020. doi:10.1115/1.4048292

obvious that the design candidates produced by using the inverse design code have overall much higher efficiency (mostly over 90%). Only a few points based on ANSYS BladeModeler have an efficiency over 90% and the Pmin value for those is relatively low. This further shows the effect of method used to parameterize the blade shape (direct or inverse) and its impact on the overall outcome of the optimization. Producing high quality DOE data will improve the efficiency of an optimization work and the computational resources won't be wasted on searching the poor design space.

CONCLUSIONS

Initially a method was presented in this paper in which the blade geometry of a high specific speed centrifugal pump impeller was parametrized by a 3D inverse design method. Both meridional shape and 3D blade shape were varied and a DOE was run by using this parametrization. The efficiency at the design point was computed by steady RANS computations while the cavitation criteria was based on minimum pressure on blade surface as computed by the 3D inverse design code. By using this approach an accurate surrogate model was obtained and this was used by an optimizer to create a good trade-off between efficiency and cavitation performance. The resulting impeller was then manufactured and tested with a retooled volute. The tests confirmed that the optimized stage has 3.9% higher efficiency than the baseline and significant improvement in suction performance.

In order to see if it is possible to further reduce computational time a slightly different optimization strategy was used, in which only the performance parameters computed by

Journal of Fluids Engineering. Received May 04, 2020;
Accepted manuscript posted August 28, 2020. doi:10.1115/1.4048292

the inverse design method were used in the optimization. So, the efficiency was correlated with profile loss and secondary flow loss and cavitation by Pmin. All parameters were computed by the inverse design method without using any expensive CFD computations. Since the inverse design method runs in a few seconds on a single core this can lead to substantial reduction in computational time. The performance of the optimized impeller geometry obtained from this process has been evaluated by CFD simulations, which show very similar efficiency and suction performance as the optimized impeller obtained by the CFD based optimization.

As a further test of the impact of blade parametrization on the results, optimization was performed by parametrizing the blade shape directly using blade angles rather than using an inverse design approach. Two different DOE were performed: one in which the blade TE angles were constrained to the value of the baseline impeller and one in which the blade TE angles were free to change. The meridional shape was varied in the same way as the inverse design optimization. All the resulting geometries were run in CFD. The results of the DOE from the direct parametrization were compared to that from the inverse design based parametrization. It is observed that DOE based on the conventional parameterization results in a much larger variation in head. Hence the data led to a less accurate surrogate model. Besides, in the conventional design the efficiency levels were generally lower than the equivalent inverse design results. The inverse design DOE concentrates the data points in the area of the design space that corresponded to higher efficiency and better cavitation performance. Therefore, by using an inverse design based optimization strategy it is possible to efficiently focus the valuable computational

Journal of Fluids Engineering. Received May 04, 2020;
Accepted manuscript posted August 28, 2020. doi:10.1115/1.4048292

resources in the part of the design space that can provide the highest possible performance.

ACKNOWLEDGMENT

The authors thank Franklin Electric Co., Inc. for permission of presenting and publishing this work.

NOMENCLATURE

Roman symbols

C_d	dissipation coefficient
DRVT	$\partial\left(r\overline{V_\theta}\right)/\partial m$
H	pump head
m	percentage meridional distance
N	number of blades
NPSH	net positive suction head
NPSHr	net positive suction head required
p	pressure
Q	pump volume flow rate
rpm	revolutions per minute
r	radius
$r\bar{V}_\theta$	circumferentially averaged bound circulation
$r\bar{V}_\theta^*$	non-dimensionalized $r\bar{V}_\theta$
$\dot{S}$	entropy generation rate
T	static temperature
V	velocity
W	meridional velocity

x	Streamwise direction

Greek symbols

δ	boundary layer thickness
θ	circumferential direction
π	$\approx 3.1415926 \ldots$
ρ	density

Superscript

$\pm$	blade pressure/suction surface

Subscript

d	design condition
LE	blade leading edge
mbl	meridional component on blade surface
mer	meridional direction
TE	blade trailing edge

REFERENCES

[1] Nelik, L., 1999, “Centrifugal & Rotary Pumps: Fundamentals with Applications,” CRC Press, Boca Raton, USA, ISBN-13: 978-1855674653.

[2] Cugal, M., Bloomfield, S., Jensen, B. M. and Jacobsen, C. B., 2009, “A Modern Pump Design Process for Higher Efficiency and Product Accuracy,” ASME 2009 Fluids Engineering Division Summer Meeting, Volume 1: Symposia, Parts A, B and C, Vail, Colorado, USA.

[3] Heo, M. W., Ma S. B., Shim H. S. and Kim K. Y., 2015, “High-efficiency design optimization of a centrifugal pump,” Journal of Mechanical Science and Technology, 30 (9) (2016) 3917~3927.

[4] Tong, S. G., Zhao, H., Liu, H. Q., Yu, Y., Li, J. F. and Cong, F. Y., 2020, “Multi-Objective Optimization of Multistage Centrifugal Pump Based on Surrogate Model,” Journal of Fluids Engineering, Vol. 142 / 011101-(1-9).

[5] Donno, R. D., Ghidoni, A., Noventa, G. and Rebay, S., 2019, “Shape optimization of the ERCOFTAC centrifugal pump impeller using open-source software,” Optimization and Engineering, (2019) 20:929–953.

[6] Wang, W. J., Osman, M. K., Pei, J., Gan, X. C. and Yin, T. Y., 2019, “Artificial Neural Networks Approach for a Multi-Objective Cavitation Optimization Design in a Double-Suction Centrifugal Pump,” Processes 2019, 7 (5), 246.

[7] Xu Y., Tan, L., Cao, S. L. and Qu, W. S., 2016, “Multiparameter and multiobjective optimization design of centrifugal pump based on orthogonal method,” Proc IMechE Part C: J Mechanical Engineering Science 2017, Vol. 231(14) 2569–2579.

[8] Wang, K., Luo, G. Z., Li, Y., Xia, R. C., Liu, H. L., 2019, “Multi-condition optimization and experimental verification of impeller for a marine centrifugal pump,” International Journal of Naval Architecture and Ocean Engineering 12 (2020) 71-84.

[9] Wang, C., Zhang, Y. X., Hou, H. C., Yuan, Z. Y. and Liu, M., 2020, “Optimization Design of an Ultra-Low Specific-Speed Centrifugal Pump Using Entropy Production Minimization and Taguchi Method,” International Journal of Fluid Machinery and Systems, Vol. 13, No. 1, January-March 2020.

[10] Shim, H. S., Kim, K. Y., Choi, Y. S., 2018, “Three-Objective Optimization of a Centrifugal Pump to Reduce Flow Recirculation and Cavitation,” Journal of Fluids Engineering, SEPTEMBER 2018, Vol. 140 / 091202-(1-14).

[11] TURBOdesign1, Version 6.6.0, 2019, Advanced Design Technology Ltd. London, UK.

[12] Zangeneh, M., 1991, “A compressible three-dimensional design method for radial and mixed flow turbomachinery blades,” International Journal for Numerical Methods in Fluids, 13 (5) 599 - 624.

[13] Dornberg, R., 2000, “Multidisciplinary Optimization in Turbomachinery Design,” European Congress on Computational Methods in Applied Sciences and Engineering, ECCOMAS 2000, Barcelona.

[14] Boniuti, D., Zangeneh, M., 2009, “On the coupling of inverse design and optimization techniques for the multi-obejective, multi-point design of turbomachinery blades,” ASME J. of Turnbomachinery, Vol 131 (2), 021014.

[15] TURBOdesign Optima, Version 6.6.0, 2019, Advanced Design Technology Ltd. London, UK.

[16] Krige, D.G, 1951, “A statistical approach to some mine valuations and allied problems at the Witwatersrand,” Master's thesis of the University of Witwatersrand, South Africa.

[17] Zangeneh, M., Goto, A. and Harada, H., 1998, “On the Design Criteria for Suppression of Secondary Flows in Centrifugal and Mixed Flow Impellers,” Journal of Turbomachinery, 120(4), 723-735.

[18] Goto, A., Zangeneh, A., Takemura, T., 1996, “Suppression of Secondary Flows in a Mixed Flow Pump Impeller by Application of 3-D Inverse Design Method,” ASME Journal of Turbomachinery, Vol. 118, pp. 544-551.

[19] Zangeneh, M., Daneshkhah, K., 2009, “A Fast 3D Inverse Design Based Multi-Objective Optimization Strategy for Design of Pumps,” ASME Fluid Engineering Division Summer Meeting Conference, At Vail, Colorado USA, Volume: FEDSM2009-7844.

[20] Goto, A., 2016, “Historical Perspective on Fluid Machinery Flow Optimization in an Industry,” International Journal of Fluid Machinery and Systems, Vol. 9, No. 1.

[21] ANSI/HI 14.6-2011, 2001, “American National Standard for Rotodynamic Pumps for Hydraulic Performance Acceptance Tests,” Hydraulic Institute, 6 Campus Drive, First Floor North, Parsippany, New Jersey 07054-4406.

[22] Denton, J. D., 1993, “Loss Mechanisms in Turbomachines,” the 1993 IGTI Scholar Lecture, Ohio USA, Journal of Turbomachinery 115(4), 621-656.

[23] Johnson, M. W., 1978, “Secondary Flows in Rotating Bends,” ASME Journal of Engineering for Power, Vol. 100. Pp. 553-560.
[24] TURBOdesign Suite, Version 6.6.0, 2019, Advanced Design Technology Ltd. London, UK.

Journal of Fluids Engineering. Received May 04, 2020;
Accepted manuscript posted August 28, 2020. doi:10.1115/1.4048292

Table Caption List

Journal of Fluids Engineering. Received May 04, 2020;
Accepted manuscript posted August 28, 2020. doi:10.1115/1.4048292

Figure Captions List

Journal of Fluids Engineering. Received May 04, 2020;
Accepted manuscript posted August 28, 2020. doi:10.1115/1.4048292

Fig. 25	Static pressure distribution on impeller blade suction surface, left: CFD optimized design; right: TD1 optimized design.
Fig. 26	Two-phase simulation at 115% design flow rate, left: baseline design; right: TD1 optimized design.
Fig. 27	The pump performance characteristics, upper: head; lower: efficiency.
Fig. 28	Beta angle distribution on a camberline, dashed line: Bezier points; solid line: fit curve.
Fig. 29	Comparison of head against Pmin for different DOEs
Fig. 30	Comparison of efficiency against Pmin for different DOEs

Journal of Fluids Engineering. Received May 04, 2020;
Accepted manuscript posted August 28, 2020. doi:10.1115/1.4048292

1	Shaft speed
2	Blade counts (6)
3	Impeller outlet diameter
4	Inlet channel height
5	Blade hub thickness
6	Blade shroud thickness
7	Volute inlet diameter/Impeller outlet diameter (1.06)
8	Volute throat area (square root)/centroid radius (0.64)

Table 1 Design parameters

Journal of Fluids Engineering. Received May 04, 2020;
Accepted manuscript posted August 28, 2020. doi:10.1115/1.4048292

Blade Parameters	**Min**	**Max**
NChub	0.17	0.45
NDhub	0.55	0.9
SLOPEhub	-1.5	2.0
DRVThub	-0.6	0.8
NCshr	0.17	0.45
NDshr	0.55	0.9
SLOPEshr	-1.5	2.0
DRVTshr	-0.6	0.6
Stacking	0	20 [deg]
RVTshroud	0.432	0.528

Table 2 Range of design variables

Journal of Fluids Engineering. Received May 04, 2020;
Accepted manuscript posted August 28, 2020. doi:10.1115/1.4048292

	Elements	Tetrahedra	Normalized Head
Coarse	469,808	243,183	1.079
Medium	2,191,764	818,287	1.076
Fine	7,630,605	1,892,476	1.075

Table 3 Mesh sensitivity study

Journal of Fluids Engineering. Received May 04, 2020;
Accepted manuscript posted August 28, 2020. doi:10.1115/1.4048292

Constraints	Objectives
Throat	Pmin (maximize)
Diffusion Ratio	Profile Loss Factor (minimize)
	Secondary Flow Factor (minimize)

Table 4 Optimization constraints and objectives used in TDOptima

Journal of Fluids Engineering. Received May 04, 2020;
Accepted manuscript posted August 28, 2020. doi:10.1115/1.4048292

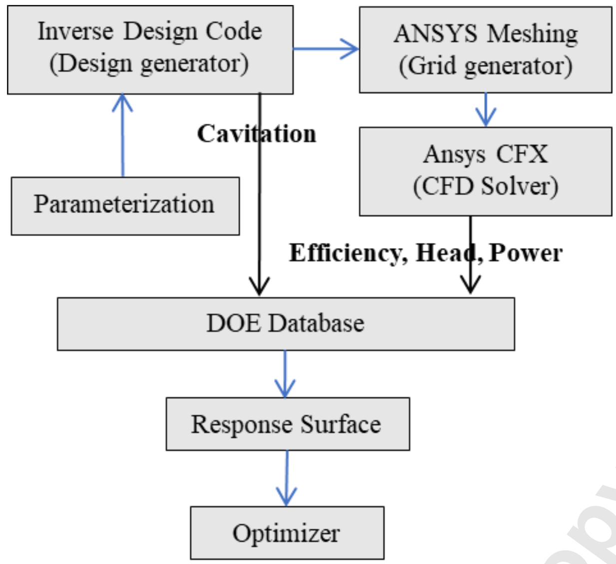

Fig. 1 Flowchart of the optimization work

Journal of Fluids Engineering. Received May 04, 2020;
Accepted manuscript posted August 28, 2020. doi:10.1115/1.4048292

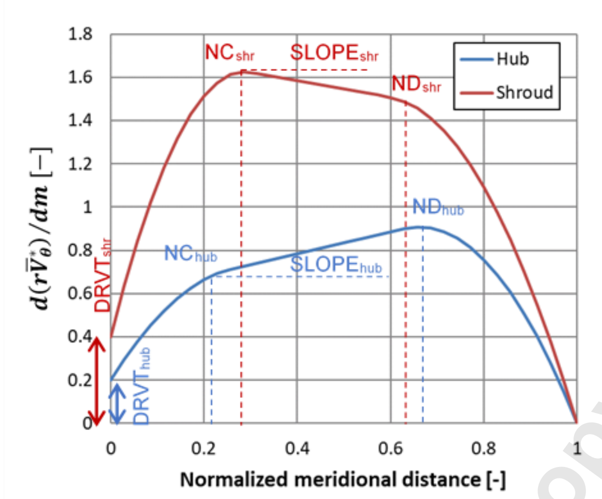

Fig. 2 The blade loading parameters used in the optimization

Journal of Fluids Engineering. Received May 04, 2020;
Accepted manuscript posted August 28, 2020. doi:10.1115/1.4048292

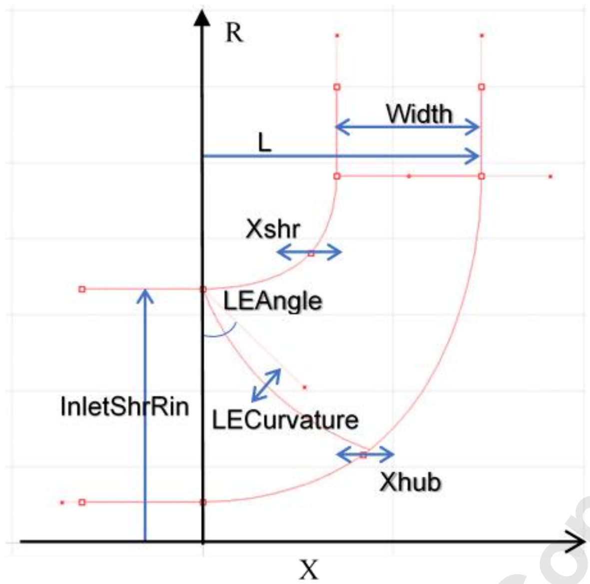

Fig. 3 Meridional parameterization

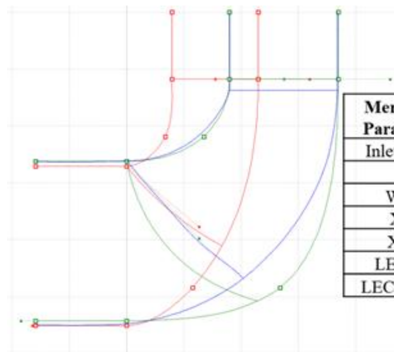

Meridional Parameters	Range
InletShrRin	-2.50%
L	-37.50%
Width	-20%
Xshr	-52%, +1.2%
Xhub	-37.2%, +1.4%
LEAngle	-4%, +1.1%
LECurvature	+166.67%, +500%

Fig. 4 Variation of meridional shape, blue: baseline; red: smallest blade area; green: largest blade area.

Journal of Fluids Engineering. Received May 04, 2020;
Accepted manuscript posted August 28, 2020. doi:10.1115/1.4048292

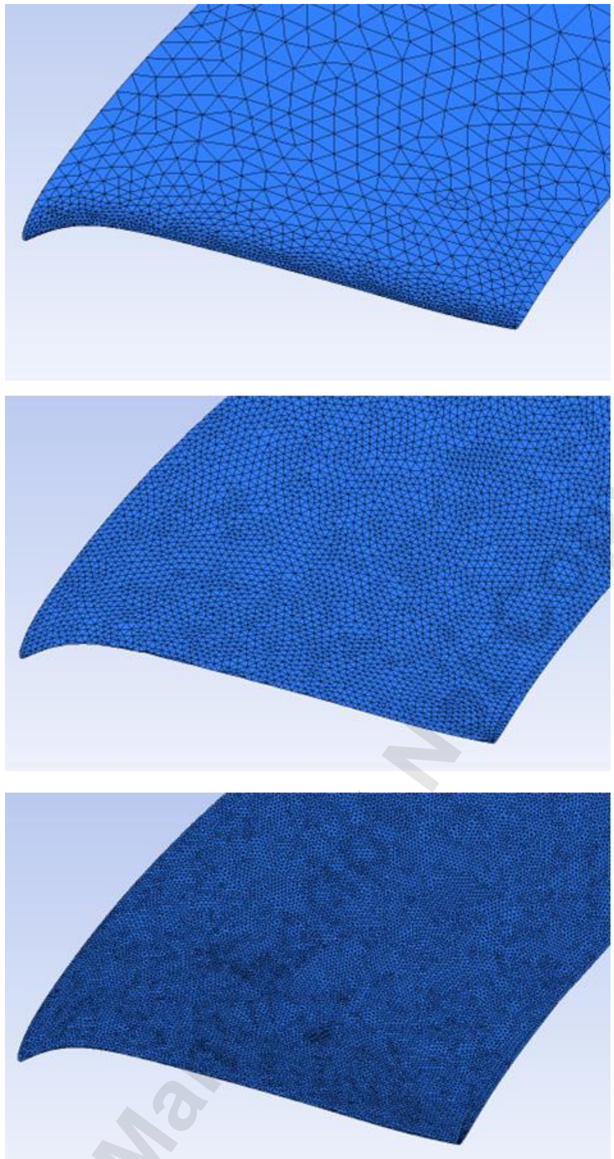

Fig. 5 Impeller surface mesh distribution, upper: coarse mesh; middle: medium mesh; lower: fine mesh.

Journal of Fluids Engineering. Received May 04, 2020;
Accepted manuscript posted August 28, 2020. doi:10.1115/1.4048292

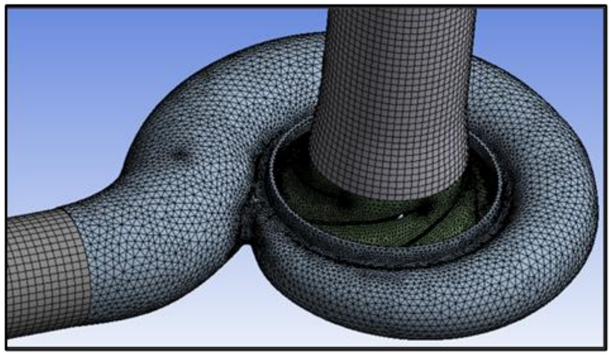

Fig. 6 Computational domain and mesh detail

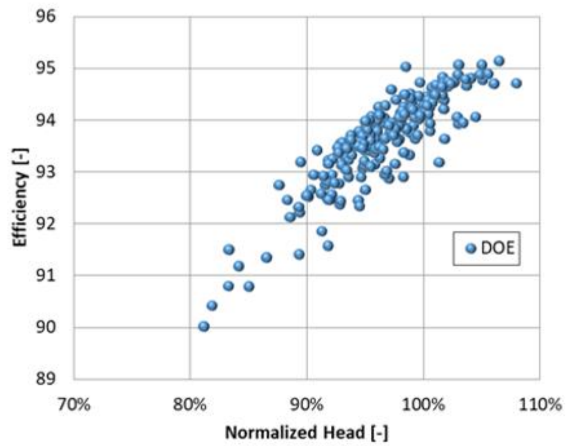

Fig. 7 Efficiency against Head of DOE results

Journal of Fluids Engineering. Received May 04, 2020;
Accepted manuscript posted August 28, 2020. doi:10.1115/1.4048292

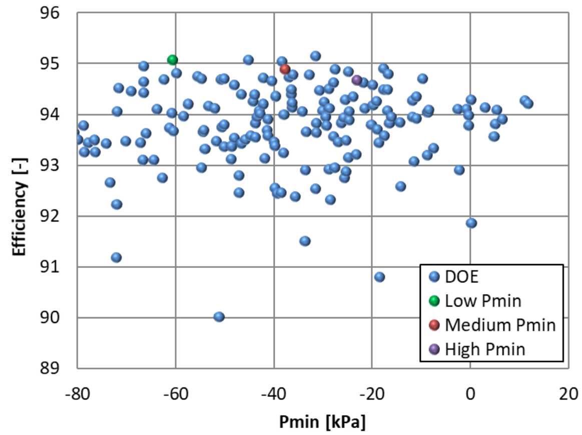

Fig. 8 Efficiency against Pmin of DOE results

Journal of Fluids Engineering. Received May 04, 2020;
Accepted manuscript posted August 28, 2020. doi:10.1115/1.4048292

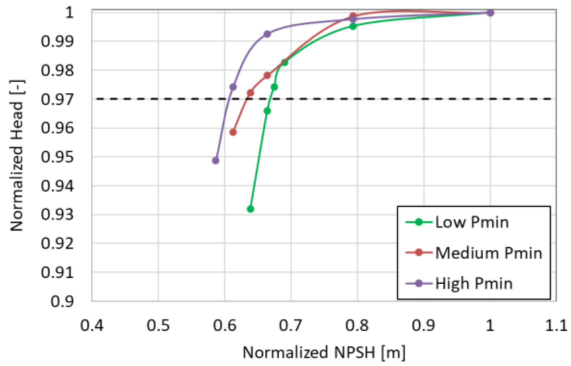

Fig. 9 Head drop curve (CFD) for designs of different Pmin at 115% design massflow

Journal of Fluids Engineering. Received May 04, 2020;
Accepted manuscript posted August 28, 2020. doi:10.1115/1.4048292

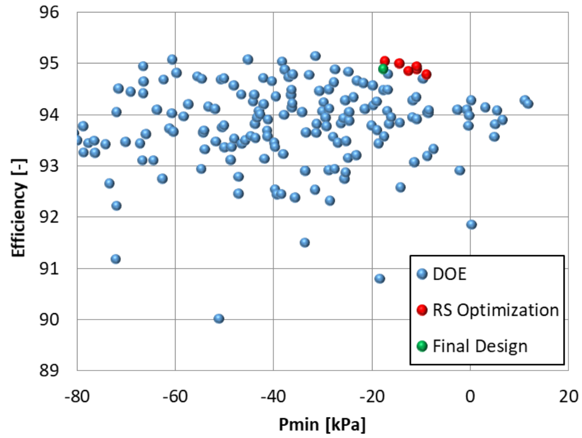

Fig. 10 Efficiency against Pmin of DOE, response surface optimization and final design.

Journal of Fluids Engineering. Received May 04, 2020;
Accepted manuscript posted August 28, 2020. doi:10.1115/1.4048292

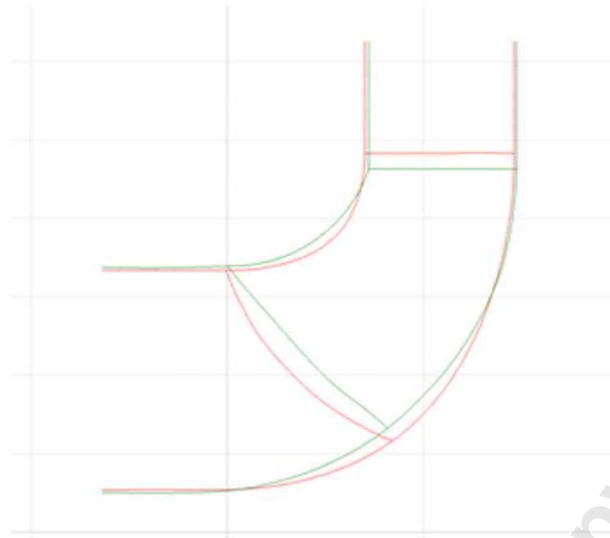

Fig. 11 Comparison of meridional profile between the baseline design (green) and the CFD optimized design (red).

Journal of Fluids Engineering. Received May 04, 2020;
Accepted manuscript posted August 28, 2020. doi:10.1115/1.4048292

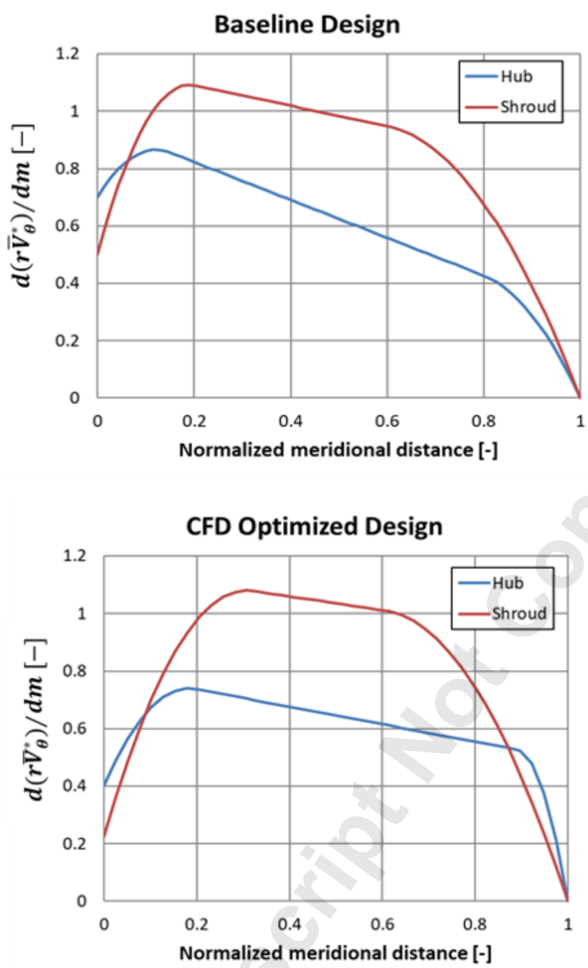

Fig. 12 Loading distribution on hub and shroud blade surface, upper: baseline design; lower: CFD optimized design.

Journal of Fluids Engineering. Received May 04, 2020;
Accepted manuscript posted August 28, 2020. doi:10.1115/1.4048292

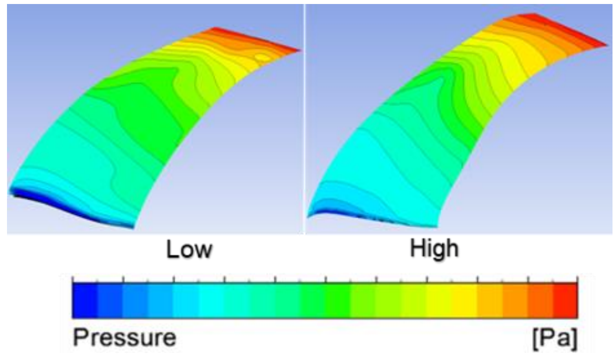

Fig. 13 Static pressure distribution on impeller blade suction surface, left: baseline design; right: CFD optimized design.

Journal of Fluids Engineering. Received May 04, 2020;
Accepted manuscript posted August 28, 2020. doi:10.1115/1.4048292

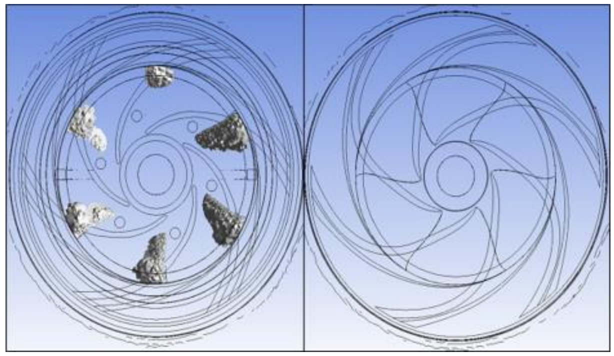

Fig. 14 Two-phase simulation at 115% design flow rate, left: baseline design; right: CFD optimized design.

Fig. 15 Prototype of the CFD optimized design

Journal of Fluids Engineering. Received May 04, 2020;
Accepted manuscript posted August 28, 2020. doi:10.1115/1.4048292

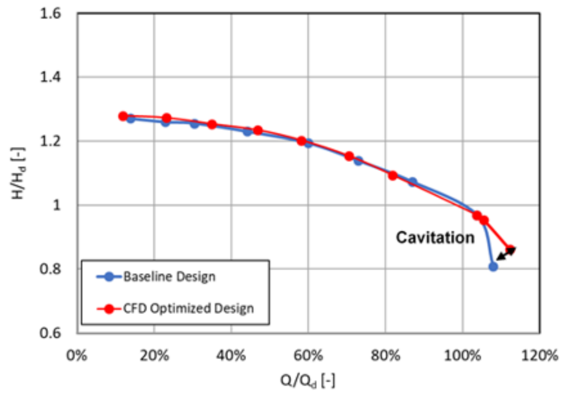

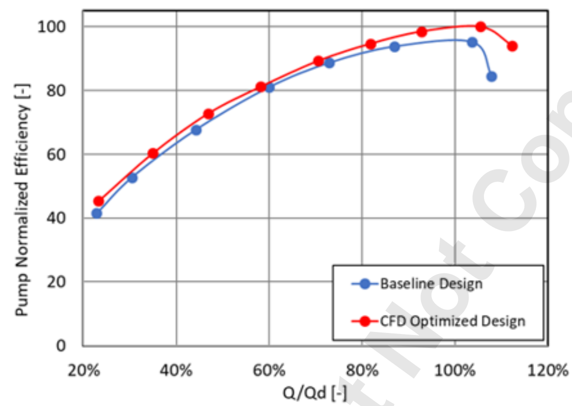

Fig. 16 Pump performance curve test data, upper: head curve; lower: pump efficiency curve.

Journal of Fluids Engineering. Received May 04, 2020;
Accepted manuscript posted August 28, 2020. doi:10.1115/1.4048292

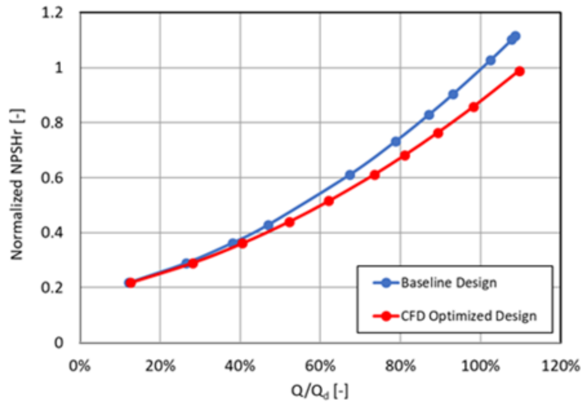

Fig. 17 Pump suction performance (normalized measured NPSHr curve) test results

Journal of Fluids Engineering. Received May 04, 2020;
Accepted manuscript posted August 28, 2020. doi:10.1115/1.4048292

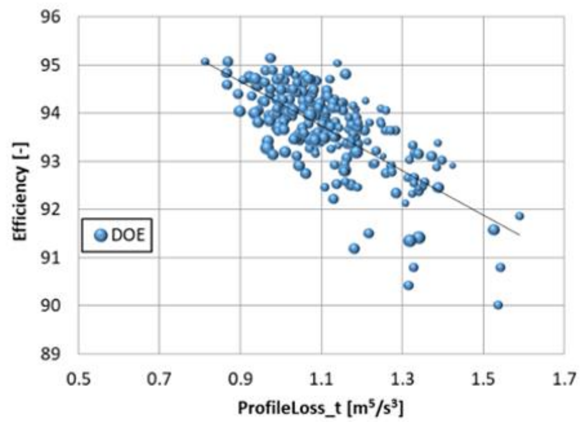

Fig. 18 Impeller efficiency against profile loss of DOE results

Journal of Fluids Engineering. Received May 04, 2020;
Accepted manuscript posted August 28, 2020. doi:10.1115/1.4048292

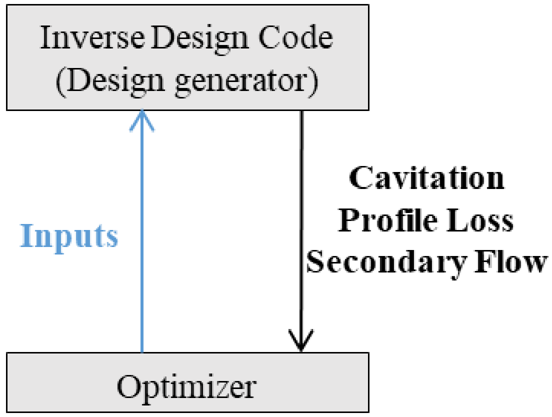

Fig. 19 Flowchart of the direct optimization

Journal of Fluids Engineering. Received May 04, 2020;
Accepted manuscript posted August 28, 2020. doi:10.1115/1.4048292

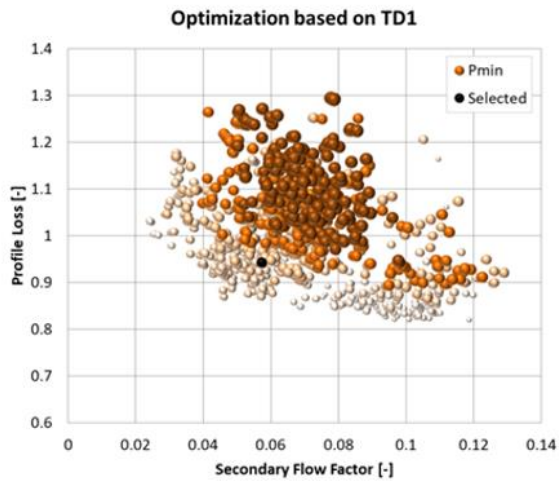

Fig. 20 Profile loss against secondary flow factor coloured by Pmin (higher Pmin points are coloured by darker and bigger bubbles).

Journal of Fluids Engineering. Received May 04, 2020;
Accepted manuscript posted August 28, 2020. doi:10.1115/1.4048292

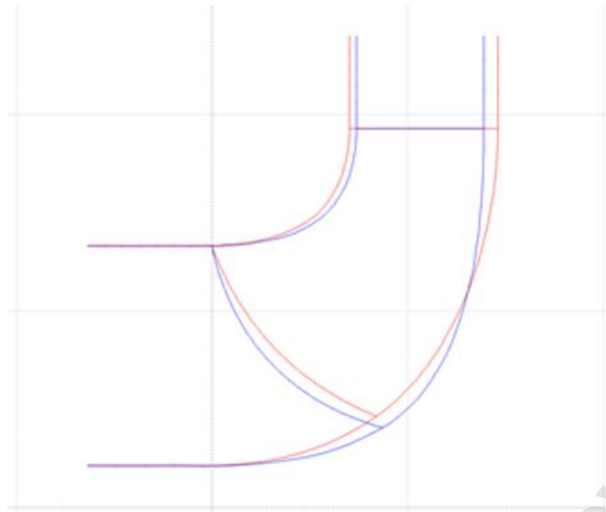

Fig. 21 Comparison of meridional profile between the CFD optimized design (red) and the TD1 optimized design (blue).

Journal of Fluids Engineering. Received May 04, 2020;
Accepted manuscript posted August 28, 2020. doi:10.1115/1.4048292

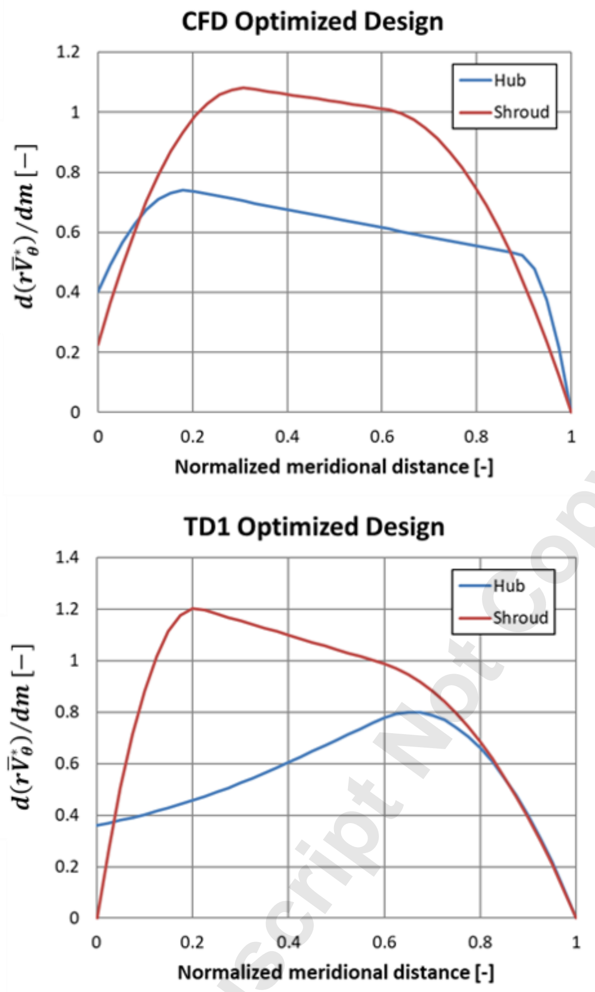

Fig. 22 Loading distribution on hub and shroud blade surface, upper: CFD optimized design; lower: TD1 optimized design.

Journal of Fluids Engineering. Received May 04, 2020;
Accepted manuscript posted August 28, 2020. doi:10.1115/1.4048292

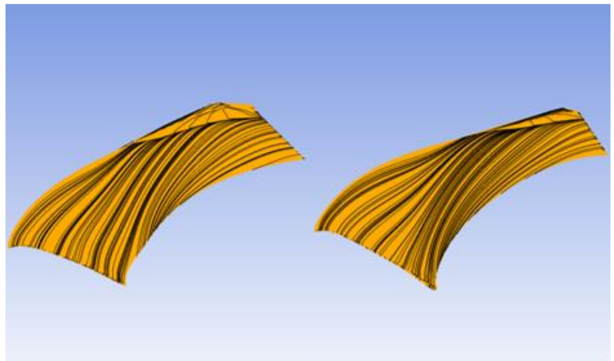

Fig. 23 Blade suction surface streamlines, left: CFD optimized design; right: TD1 optimized design.

Journal of Fluids Engineering. Received May 04, 2020;
Accepted manuscript posted August 28, 2020. doi:10.1115/1.4048292

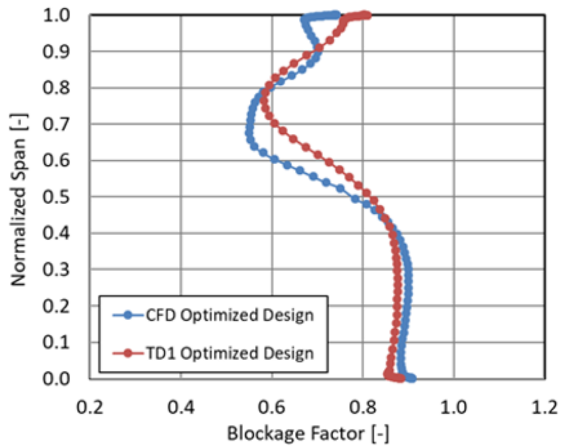

Fig. 24 Spanwise distribution of blockage factor ($\frac{\overline{V_{mer}^{area}}}{\overline{V_{mer}^{mass}}}$)

Journal of Fluids Engineering. Received May 04, 2020;
Accepted manuscript posted August 28, 2020. doi:10.1115/1.4048292

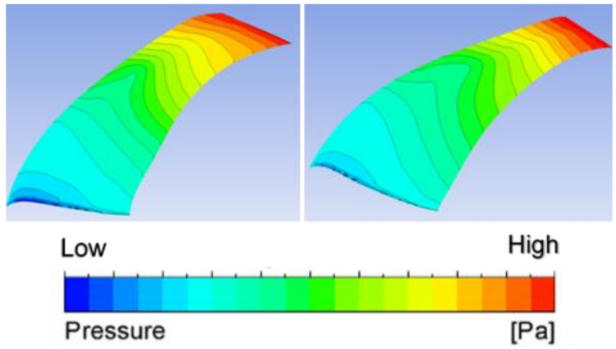

Fig. 25 Static pressure distribution on impeller blade suction surface, left: CFD optimized design; right: TD1 optimized design.

Journal of Fluids Engineering. Received May 04, 2020;
Accepted manuscript posted August 28, 2020. doi:10.1115/1.4048292

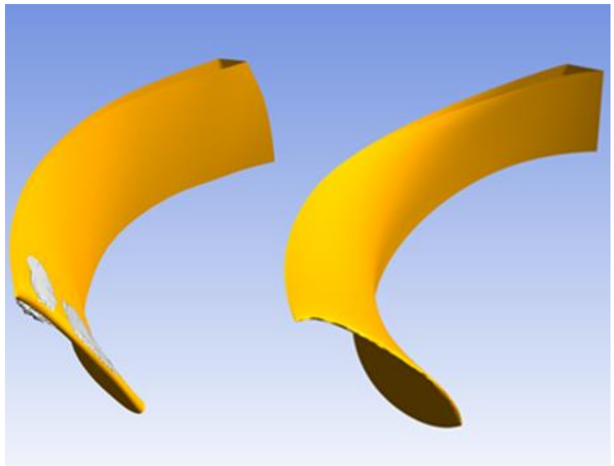

Fig. 26 Two-phase simulation at 115% design flow rate, left: baseline design; right: TD1 optimized design.

Journal of Fluids Engineering. Received May 04, 2020;
Accepted manuscript posted August 28, 2020. doi:10.1115/1.4048292

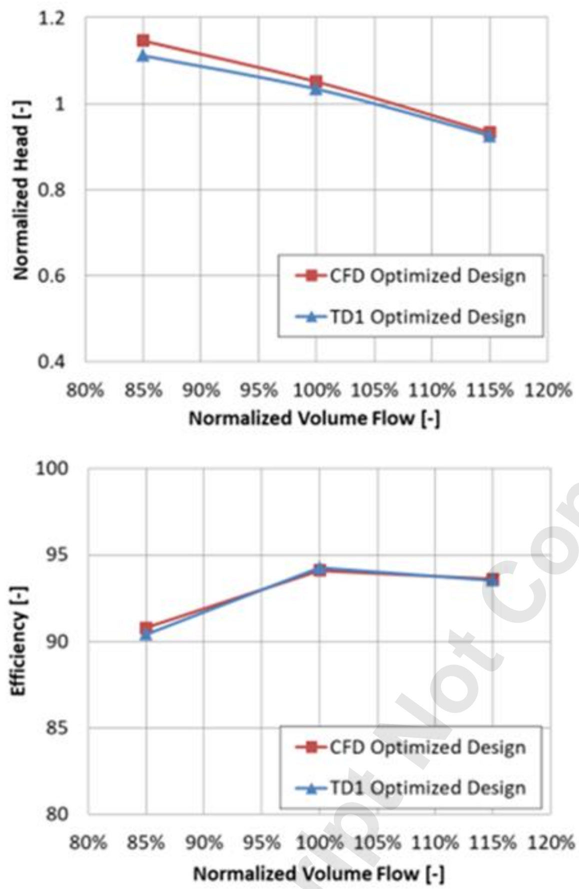

Fig. 27 The pump performance characteristics, upper: head; lower: efficiency.

Journal of Fluids Engineering. Received May 04, 2020;
Accepted manuscript posted August 28, 2020. doi:10.1115/1.4048292

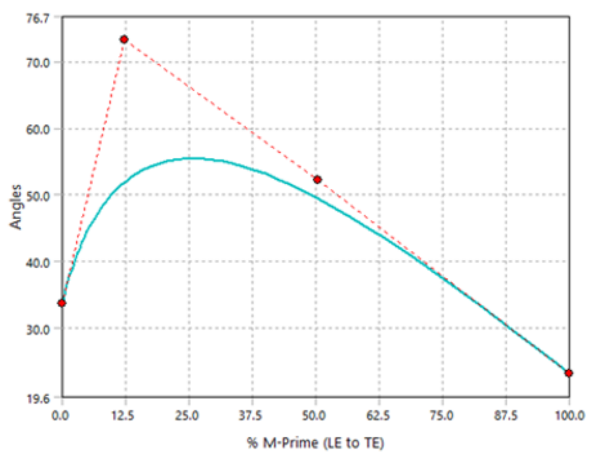

Fig. 28 Beta angle distribution on a camberline, dashed line: Bezier points; solid line: fit curve.

Journal of Fluids Engineering. Received May 04, 2020;
Accepted manuscript posted August 28, 2020. doi:10.1115/1.4048292

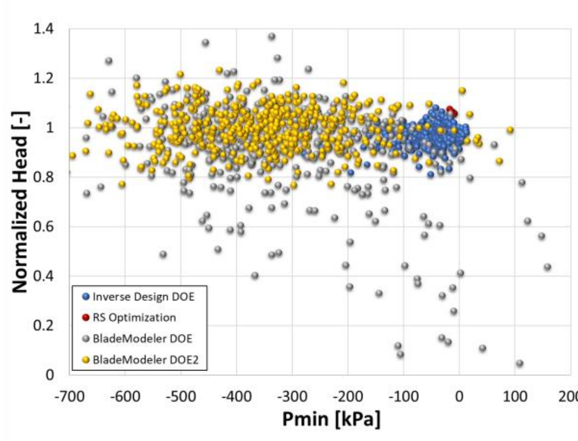

Fig. 29 Comparison of head against Pmin for different DOEs

Journal of Fluids Engineering. Received May 04, 2020;
Accepted manuscript posted August 28, 2020. doi:10.1115/1.4048292

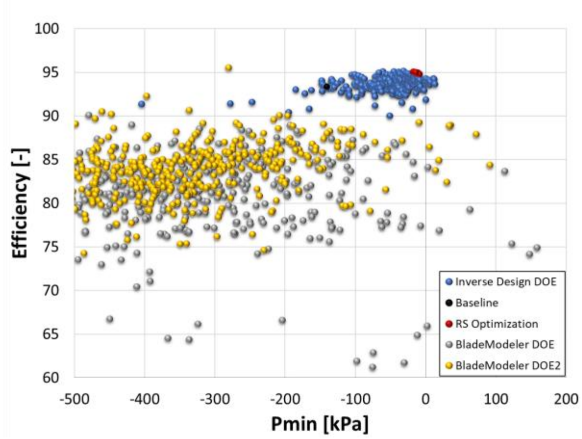

Fig. 30 Comparison of efficiency against Pmin for different DOEs